Electronic states in doped conducting polymers: Numerical simulation of disordered systems

Kikuo Harigaya, Akira Terai, and Yasushi Wada
Department of Physics, University of Tokyo, Bunkyo-ku, Tokyo 113, Japan

Klaus Fesser
Physikalisches Institut, Universität Bayreuth, D-8580 Bayreuth, Federal Republic of Germany
(Received 21 June 1990; revised manuscript received 27 August 1990)

In order to substantiate the applicability of the coherent-potential approximation (CPA) to conducting polymers with randomly distributed impurities, the Su-Schrieffer-Heeger model is generalized by including the effects of the impurities and solved numerically. The lattice configurations, electronic levels, and wave functions are determined for each impurity distribution. The size of lattice dimerization and electronic density of states are determined and averaged over a large number of impurity distributions, which are selected independently and randomly. The study is confined to systems with one electron per site that we have studied previously using the CPA. Two types of impurities as well as three doping mechanisms are considered. It turns out that the magnitude of lattice dimerization agrees remarkably well with the CPA result for all impurity types and doping mechanisms under consideration. The density of states shows a characteristic tail at the edge of a band where the CPA predicts an impurity band at lower concentrations. Such a tail never occurs in regimes where the CPA does not predict such bands. Quasilocalization is found in the wave functions of the states at the band edges. It is closely associated with the characteristic structure of the density of states. The usefulness of the CPA is thus established for the Peierls system as far as gross qualitative properties are concerned.

I. INTRODUCTION

In a series of papers[1–6] we have been investigating the effects of random impurities on the electronic properties of conjugated polymers. Two types of impurities have been studied. One is the site-type impurity which locally varies the site energy of π electrons. The other is the bond-type impurity which locally changes the electronic transfer integral. The Su-Schrieffer-Heeger (SSH) Hamiltonian[7] has been generalized to include the effects of these impurities.

It is possible to carry out analytical investigations, using the continuum limit [Takayama–Lin-Liu–Maki (TLM) model[8,9]] of the generalized SSH Hamiltonian. The one-dimensional lattice of the SSH model is dimerized when there is one electron per site. If the bond between the $2n$th site and the neighboring $(2n+1)$th site is short, we have a long bond between the $(2n+1)$th site and the $(2n+2)$th site, and vice versa. This pattern extends over the chain. A site-type impurity at an even-numbered site gives a different effect on electrons from a site-type impurity at an odd-numbered site. Similarly, a bond-type impurity along a short bond gives a different effect from an impurity along a long bond. These differences persist in the continuum limit.

We have been interested in the formation of impurity bands in the gap, the change in the order parameter, and a possible vanishing of the energy gap. These properties have been investigated with the help of the Soven-Taylor coherent-potential approximation (CPA). It is a method which is convenient to study such properties and would give reliable results as far as gross and qualitative information are concerned. We have so far confined the study to a system with uniform order parameter and half-filled electronic states.

The bond-type impurity effects have been investigated in Refs. 2 and 4. To simplify the analysis in Ref. 2, the impurity along a short bond is assumed to give an opposite effect on the electron transfer to the impurity along a long bond. When the former enhances the transfer, the latter deemphasizes it by the same amount, and vice versa. The enhancement pattern is, therefore, in phase with the dimerization. We shall later name these impurities *cis*-type. It has been found that there is no impurity band in the energy gap. In Ref. 4, each impurity has been supposed either to enhance or deemphasize the transfer with an equal probability. Half of the impurities are in phase with the dimerization and the other half are out of phase. Two impurity bands can be formed through the out-of-phase impurities. This type of disorder would take place when a bond is shortened or elongated by a possible local misalignment with neighboring impurity and polyacetylene chains.

The site-type impurity problems have been studied in Refs. 3–5. In Ref. 3 we have investigated the impurity distribution in which the impurities are at interstitial sites either always along the long bonds or always along the short bonds. Each impurity modifies the electronic site

energy at the two ends of the bond by the same amount. This would be the case when the impurity is charged, releasing an electron to or accepting it from another chain. It modifies the site energy strongly.[1] This distribution simplifies the problem since it eliminates backward scatterings of electrons. At low concentrations, an isolated impurity band is formed above the top of the valence band or below the bottom of the conduction band according to the sign of the impurity strength. At high concentrations and large impurity strengths, the order parameter and energy gap vanish. In the succeeding paper,[5] another impurity distribution is studied. Each impurity is assumed to be located at a lattice site. Half of them are at the even-numbered sites and the other half at the odd-numbered sites. They give rise to backward as well as forward scattering. There are no qualitative changes from the results of Ref. 3. This indicates that the analysis, developed in Ref. 3 for the interstitial distribution, does give the qualitative features of various distributions of site-type impurities correctly. The situation becomes a little complex when the doping is compensated with the same amount of donors as acceptors being introduced. The former gives rise to attractive potentials to the electrons, while the latter gives repulsive potentials. In Ref. 4 they are assumed to occupy the interstitial sites as in Ref. 3. At low concentrations we have found two impurity bands, one of them being closer to the valence band and the other to the conduction band. Even this structure can be understood with the help of the results in Ref. 3. Since there are impurities with different signs, one impurity band is formed by the impurities with one sign and the other band is formed by the other impurities with the other sign.

In general, the impurities would modify the electronic transfer integral and the site energy at the same time. It has been pointed out in Ref. 1 that, at low concentrations, the formation of impurity bands is suppressed when the strength of the bond component is larger than that of the site component. At high concentrations[6] the energy gap does vanish for strong site components. As the bond component stabilizes the dimerization, it becomes more difficult to disrupt the energy gap so as to gain the electronic energy.

These results are very fertile and quite interesting. There are, however, two problems which we have to discuss. One of them is the fact that the energy gap vanishes at higher concentrations and stronger impurity strengths than the experimentally observed concentrations and strengths, respectively. This problem will be studied in a separate paper. The other problem is the question of how reliable the CPA results are, particularly when applied to low-dimensional systems.

The purpose of this paper is to answer this question by numerical investigations of the electronic level structure of the generalized SSH model. The method of the numerical investigation was developed independently by Sun, Wu, and Shen,[10] Chao and Wang,[11] and one of the present authors and Ono[12] for the SSH model without impurities. The equation for the electronic wave functions is solved depending on the order parameter. The order parameter is, in turn, determined with the help of the wave functions. The whole problem is thus solved by an iteration. The lattice vibrations around solitons and polarons were investigated by this method, including systems with electron-electron interactions[13] and with site-type and bond-type impurities.[14] Soliton formation and pinning were demonstrated and infrared activities of localized phonons around the soliton were studied. Information on the electronic density of states could have been derived and used in the calculations, but they were not taken out of the numerical procedures. In the present study we extract the electronic properties as the density of states and wave functions in order to see if they can reproduce the features predicted by the CPA.

Since the impurities are assumed to be distributed randomly, an average over this distribution has to be performed for physical quantities which are numerically obtained for each distribution. We select $N_{\rm sa}$ samples which are determined independently. In each sample, the positions of the impurities are selected randomly. Such physical quantities as the dimerization amplitude and the electronic density of states are averaged over the $N_{\rm sa}$ samples. In the present work, $N_{\rm sa}$ is taken to be 100.

We confine the study to systems with one electron per site in accordance with the previous CPA studies. In other words, we consider the effects of isoelectronic disorder generated by the dopants. In order to obtain maximal information from the numerical results with a system of finite size, we use a generalized, quasiperiodic, boundary condition for the electronic wave functions.[15] The wave functions do not have the same value at the two ends of the system, but differ by a constant phase factor. Our system is effectively regarded as a unit of a larger system. It can give energy eigenvalues between a pair of the successive eigenvalues of the original system. In addition, we can measure the degree of localization of the wave functions by varying the phase. The eigenvalue does not change if the corresponding wave function is localized, since in this case it is not affected by the boundary condition.

In each doping method we choose a typical sample for which we show lattice configurations, electron density distributions, and the wave functions near the energy gap. The averaging procedures are performed to obtain the order parameter and density of states, and they are compared with the CPA results. We find remarkable agreements when impurity concentrations are as low as several percent. It suggests the reliability of the CPA as far as the qualitative features of the physical quantities are concerned.

Furthermore, we find that the wave functions tend to localize according to the sign of impurity potentials with the site-type impurities. In the case of the bond type, on the other hand, they have large amplitudes in regions where the order parameter becomes relatively small.

In Sec. II the impurity models are presented within

the SSH model, and the relations to the TLM model are explained. The numerical method is briefly summarized. Section III is devoted to the numerical results for the systems with site-type impurities. Section IV is for bond-type impurities. The discussions follow in Sec. V.

II. MODEL AND NUMERICAL METHOD

The generalized SSH Hamiltonian is taken to be

$$H = H_{\rm SSH} + H_{\rm imp} \ , \tag{2.1}$$

where the first term is the SSH Hamiltonian

$$H_{\rm SSH} = -\sum_{n,s}[t_0 - \alpha(u_{n+1} - u_n)](c^{\dagger}_{n+1,s}c_{n,s} + \text{H.c.}) + \frac{K}{2}\sum_n (u_{n+1} - u_n)^2 \ . \tag{2.2}$$

Here $c_{n,s}$ is an annihilation operator of an electron at the nth site with spin s, t_0 the nearest-neighbor transfer integral of an undimerized chain, u_n the displacement of the nth CH unit, and K the force constant between the adjacent units. The quantity α characterizes the electron-phonon coupling strength due to the modulation of the transfer integral. The second term in (2.1) is given by the impurities. The site-type impurities give

$$H_{\rm imp} = I_s \sum_{i,s} c^{\dagger}_{i,s}c_{i,s} \ , \tag{2.3}$$

where the sum with respect to i is taken over all the impurity sites which are distributed randomly. The parameter I_s is the impurity strength. In the continuum limit, Eq. (2.3) becomes[9]

$$H_{\rm imp} = U_s \sum_s \int dx \Psi^{\dagger}_s(x)\delta(x - x_i^{(+)})(1+\sigma_2)\Psi_s(x) + U_s \sum_s \int dx \Psi^{\dagger}_s(x)\delta(x - x_i^{(-)})(1-\sigma_2)\Psi_s(x) \ , \tag{2.4}$$

where $\Psi_s(x)$ is the two component operator in the TLM model, and $U_s = aI_s$, a being the lattice constant; $x_i^{(+)}$ indicates a position of an impurity at an even-numbered site, while $x_i^{(-)}$ at an odd-numbered site; Pauli matrices are denoted by σ_i $(i = 1,2,3)$. When any two adjacent sites are occupied by the impurities, the continuum limit cannot be represented by (2.4). At low-impurity concentrations, however, effects of such impurity pairs would be small and can be neglected. The model (2.4) has been studied in Ref. 5 with the help of the CPA. The quantities I_s and U_s have been denoted by $2J$ and U there.

The generalized SSH Hamiltonian (2.1) gives an equation for the electronic wave function

$$\varepsilon_\mu \phi_\mu(n) = -(t_0 - \alpha y_{n-1})\phi_\mu(n-1) - (t_0 - \alpha y_n)\phi_\mu(n+1) + I_s \sum_i \delta_{i,n}\phi_\mu(n) \ , \tag{2.5}$$

where $y_n = u_{n+1} - u_n$ and ε_μ an eigenvalue. The function y_n is determined by

$$y_n = -\frac{\alpha}{K}{\sum_{\mu,s}}' [\phi^*_\mu(n+1)\phi_\mu(n) + \phi^*_\mu(n)\phi_\mu(n+1)] + \frac{\alpha}{KN}\sum_m {\sum_{\mu,s}}' [\phi^*_\mu(m+1)\phi_\mu(m) + \phi^*_\mu(m)\phi_\mu(m+1)] \ , \tag{2.6}$$

where the prime indicates that the sum is taken over occupied states. The second term is added to satisfy the condition $\sum_n y_n = 0$.

In order to obtain maximal information from the simulation of a small system, we make use of a kind of Bloch's theorem for electron states in a periodic lattice.[15] Suppose the computations are to be carried out on a system of N lattice sites. We regard this as a unit cell of the crystal in Bloch's theorem. Our total system is composed of many such unit cells. The theorem, then, states that the electron wave functions satisfy

$$\phi_\mu(n+N) = e^{i\theta}\phi_\mu(n) \ , \tag{2.7}$$

where θ/N is a Bloch momentum, μ being a quantum number. It is well known that the wave function can be written

$$\phi_\mu(n) = \exp(i\theta n/N)\psi_\mu(n) \ , \tag{2.8}$$

in terms of a periodic function which satisfies

$$\psi_\mu(n+N) = \psi_\mu(n) \ . \tag{2.9}$$

Since the lattice displacements u_n determine the potential in the cell, they have to satisfy the ordinary periodic boundary condition

$$u_n = u_{n+N} \ . \tag{2.10}$$

Substituting (2.8) into (2.5), we get

$$\varepsilon_\mu \psi_\mu(n) = -(t_0 - \alpha y_{n-1})e^{-i\theta/N}\psi_\mu(n-1) - (t_0 - \alpha y_n)e^{i\theta/N}\psi_\mu(n+1) + I_s \sum_i \delta_{i,n}\ \psi_\mu(n) \ , \tag{2.11}$$

and Eq. (2.6) becomes

$$\begin{aligned} y_n &= -\frac{\alpha}{K}{\sum_{\mu,s}}' [e^{i\theta/N}\psi^*_\mu(n+1)\psi_\mu(n) + e^{-i\theta/N}\psi^*_\mu(n)\psi_\mu(n+1)] \\ &\quad + \frac{\alpha}{KN}\sum_m {\sum_{\mu,s}}' [e^{i\theta/N}\psi^*_\mu(m+1)\psi_\mu(m) + e^{-i\theta/N}\psi^*_\mu(m)\psi_\mu(m+1)] \\ &= -\frac{2\alpha}{K}{\sum_{\mu,s}}' \text{Re}[e^{i\theta/N}\psi^*_\mu(n+1)\psi_\mu(n)] + \frac{2\alpha}{KN}\sum_m {\sum_{\mu,s}}' \text{Re}\ [e^{i\theta/N}\psi^*_\mu(m+1)\psi_\mu(m)] \ . \end{aligned} \tag{2.12}$$

When impurities are bond type, we first consider the model

$$H_{\rm imp} = I_b \sum_{i,s} (-1)^i (c^\dagger_{i,s} c_{i+1,s} + c^\dagger_{i+1,s} c_{i,s}) \ . \tag{2.13}$$

The impurity along a short bond gives an opposite effect to the impurity along a long bond. Its continuum limit is

$$H_{\rm imp} = U_b \sum_{i,s} \int dx \Psi^\dagger_s(x)\ \delta(x - x_i) \sigma_1 \Psi_s(x) \ , \tag{2.14}$$

where $U_b = 2aI_b$. This was studied in Ref. 2, using the CPA. Since Brazovskii and Kirova[16] used a version of homogeneous distribution of (2.14) to describe the *cis*-polyacetylene, we name the doping with impurities (2.14) *cis*-type doping, hereafter.

We next study another model

$$H_{\rm imp} = \sum_{i,s} (-1)^i [I_b \xi^{(+)}_i + (-I_b)\ \xi^{(-)}_i] \times (c^\dagger_{i,s} c_{i+1,s} + c^\dagger_{i+1,s} c_{i,s}) \ , \tag{2.15}$$

where the quantities $\xi^{(\pm)}_i$ are random variables which satisfy

$$\xi^{(\pm)}_i = \begin{cases} 1, & \text{if there is an impurity at the } i\text{th site with the potential} \\ & \text{strength } (-1)^i(\pm I_b), \text{ respectively,} \\ 0, & \text{otherwise .} \end{cases} \tag{2.16}$$

There are as many $\xi^{(+)}$-impurities as $\xi^{(-)}$-impurities corresponding to donors and acceptors, respectively. We name this doping compensated doping. Its continuum limit is

$$H_{\rm imp} = U_b \sum_{i,s} \int dx \Psi^\dagger_s(x) \delta(x - x^{(+)}_i) \sigma_1 \Psi_s(x) + (-U_b) \sum_{i,s} \int dx \Psi^\dagger_s(x) \delta(x - x^{(-)}_i) \sigma_1 \Psi_s(x) \ , \tag{2.17}$$

which was discussed in Ref. 4 by the CPA. The electron wave functions are determined by

$$\varepsilon_\mu \psi_\mu(n) = [-(t_0 - \alpha y_{n-1}) + I_b \sum_i \delta_{i,n-1} (-1)^{n-1}] e^{-i\theta/N} \psi_\mu(n-1) + [-(t_0 - \alpha y_n) + I_b \sum_i \delta_{i,n} (-1)^n] e^{i\theta/N} \psi_\mu(n+1) \ , \tag{2.18}$$

for the *cis*-type doping and by

$$\varepsilon_\mu \psi_\mu(n) = [-(t_0 - \alpha y_{n-1}) + I_b \sum_i (\xi^{(+)}_i - \xi^{(-)}_i) \delta_{i,n-1} (-1)^{n-1}] e^{-i\theta/N} \psi_\mu(n-1) + [-(t_0 - \alpha y_n) + I_b \sum_i (\xi^{(+)}_i - \xi^{(-)}_i) \delta_{i,n} (-1)^n] e^{i\theta/N} \psi_\mu(n+1) \ , \tag{2.19}$$

for the compensated doping.

To perform numerical computations, we choose $N_{\rm imp}$ sites out of N total sites at random. We thus fix a set of impurity sites i. An initial set of the bond variables $\{y^{(0)}_n\}$ is taken to be $y^{(0)}_n = (-1)^n y_0$. Since the preceding CPA studies have considered systems with one electron per site and assumed a uniform order parameter, this initial set would qualitatively correspond to this assumption, although we take into account small deviations from this set in the present computations. Then we start iterations. At the kth step, the eigenvalue equation is solved, using the $(k-1)$th set of $\{y^{(k-1)}_n\}$, and the obtained eigenfunctions are used to get the kth set of $\{y^{(k)}_n\}$. The iteration is repeated until the sum $\sum_n (y^{(k)}_n - y^{(k-1)}_n)^2$ becomes sufficiently small.

III. SITE-TYPE IMPURITIES

A. A typical solution

In the numerical studies we use the parameters $\alpha = 4.1$ eV/Å, $K = 21$ eV/Å^2, and $t_0 = 2.5$ eV for the system with $N_{\rm el} = N = 100$, $N_{\rm el}$ being the total number of electrons. These give the dimensionless electron-phonon coupling constant $\lambda \equiv 2\alpha^2/\pi K t_0 = 0.20$. All the quantities with the dimension of energy are given in units of t_0. The initial value of the lattice displacement is $y_0 = -0.1$ Å. This choice should be reasonable since its absolute value is about 0.08 Å in the impurity-free system.

In this subsection we show a typical solution, when the impurity strength is $I_s = 0.4t_0$ and the concentration $c = 0.08$. In Fig. 1(a) a set of the smoothed dimerization amplitude $\bar{y}_n = (-1)^n (y_n - y_{n+1})/2$ is plotted as a function of n. Positions of impurities are denoted by squares on the abscissa. The phase in (2.7) is taken as $\theta = 0$. In Fig. 1(b), the electron-density distribution is plotted, after the smoothing procedure $\bar{\rho}_n = (\rho_{n-1} + 2\rho_n + \rho_{n+1})/4$. Around each impurity, the dimerization amplitude becomes small. It deforms asymmetrically with respect to the position of the impurity. The electron density decreases at the impurity site due to the repulsive impurity potential I_s. Its distribution is asymmetric also. It decreases on one side and increases on the other. The

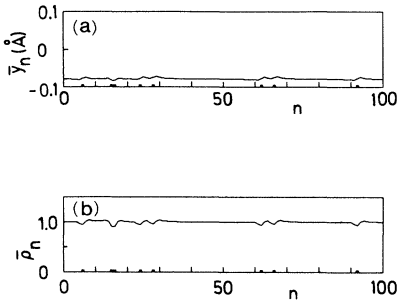

FIG. 1. (a) The smoothed dimerization amplitude, $\bar{y}_n = (-1)^n(y_n - y_{n+1})/2$, and (b) the smoothed electron-density distribution, $\bar{\rho}_n = (\rho_{n-1} + 2\rho_n + \rho_{n+1})/4$, for a typical sample with site-type impurities. The impurity strength is $I_s = 0.4t_0$, and the concentration $c = 0.08$. The phase θ is zero. Positions of the impurities are indicated by squares on the abscissa. The average electron density over the whole sample is unity.

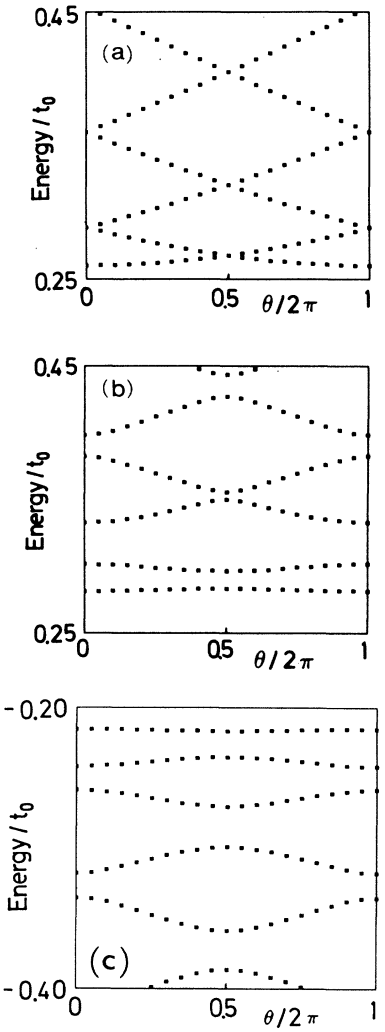

FIG. 2. The energy eigenvalues of the electronic states as functions of the phase θ. (a) The lowest six eigenvalues of the conduction band of the impurity-free system. (b) gives the six eigenvalues at the bottom of the conduction band of the typical sample shown in Fig. 1. (c) shows the eigenvalues at the top of the valence band.

asymmetry is due to the fact that there is a short bond on one side and a long bond on the other side of the impurity. At the short bond, the transfer integral is larger than t_0. The larger transfer integral generates a longer tail of increased electron density. At the long bond, on the other hand, the transfer integral is smaller. It generates a shorter tail of the decreased electron density.

The θ dependence of the electronic eigenvalues ε_μ is shown in Fig. 2. Figure 2(a) shows the lowest six eigenvalues of the conduction band in the impurity-free system. The results at $\theta = 0$ and π correspond to systems with periodic and antiperiodic boundary conditions, respectively. The eigenvalues are pairwise degenerate. When θ is neither zero nor π, this degeneracy is removed and the eigenvalues vary monotonously. This shows that eigenfunctions extend over the system (they are plane waves). Figures 2(b) and 2(c) show the θ dependences of the eigenvalues at the bottom of the conduction band and the top of the valence band for the doped system discussed in Fig. 1, respectively. The pairwise degeneracy in Fig. 2(a) is removed. The θ dependences are weaker compared with Fig. 2(a). This means that the wave functions are more or less affected by the disorder potential to have large amplitudes around particular regions in space.

Figure 3(a) shows the magnitude of four wave functions $|\psi_\mu(n)|^2$ at the top of the valence band and the bottom of the conduction band. The electronic states are numbered in the order of magnitude of the eigenvalues. The states of the valence band are numbered in $1 \leq \mu \leq N/2$. Those of the conduction band have the numbers $N/2 + 1 \leq \mu \leq N$. Figure 3(a) is for $\mu = 49$

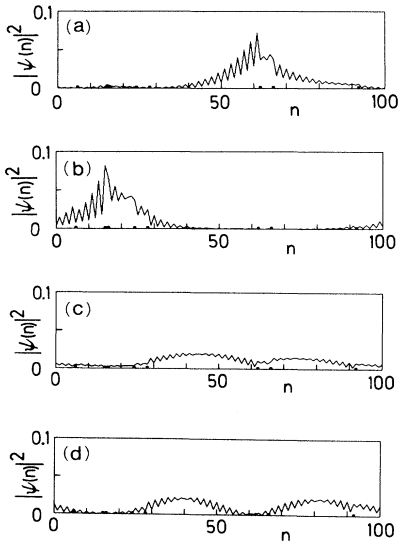

FIG. 3. Magnitude of the wave functions $|\psi_\mu(n)|^2$ for the typical sample in Fig. 1. (a) is for $\mu = 49$ and (b) for $\mu = 50$ (the top of the valence band). (c) is for $\mu = 51$ and (d) for $\mu = 52$ (the bottom of the conduction band).

and Fig. 3(b) for $\mu = 50$, corresponding to valence-band states with second highest and highest energy, respectively. Figure 3(c) is for $\mu = 51$ and Fig. 3(d) for $\mu = 52$, i.e. lowest and next lowest energy conduction-band states. The wave functions at the top of the valence band have large amplitudes around the impurity sites, while those at the bottom of the conduction band prefer to localize in the impurity-free regions. This is because I_s is positive. In general, we find that the states at the upper edge of a certain band tend to localize around impurities, while the states at the bottom of the same band have large amplitudes in the impurity-free regions.

B. Averaged data

The typical solution, discussed in the previous subsection, has to be averaged over various impurity distributions, that is, over various samples.

The bond variable y_n is averaged over N sites and $N_{\rm sa}$ samples. We take $N_{\rm sa} = 100$. The averaged value is $\langle | y_n | \rangle = 0.0780$ Å. This gives the order parameter in the TLM model $\Delta \equiv 2\alpha \langle | y_n | \rangle = 0.640$ eV$= 0.256t_0$. In the CPA investigations the continuum Hamiltonians (2.4), (2.14), and (2.17) are used. To solve the CPA equations numerically, we have replaced the continuum system by a discrete system. The lattice constant of the discrete system has been taken to be $2a$ which is the size of the unit cell of the dimerized system. The strength of the impurity potential is defined by $J \equiv U_s/2a = I_s/2$, and is thus half as large as the strength in the SSH model. This comes from the fact that in the CPA the lattice unit is doubled. On the other hand, the impurity concentration becomes twice as large as that of the SSH model, since it is the average number of the impurities in the unit cell. Our typical solution is given for $I_s = 0.4t_0$ and $c = 0.08$, which corresponds to $J = 0.2t_0$ and $c_{\rm CPA} = 0.16$ in Ref. 5. The concentration in the CPA analyses will be denoted by $c_{\rm CPA}$, hereafter: $c_{\rm CPA} = 2c$. Although the order parameter has not been explicitly given for this strength in Ref. 5, its value is $\Delta = 0.639$ eV $= 0.255t_0$. The coupling constant has been taken to be $\lambda = 0.183$, which has led to the order parameter in the impurity-free system $\Delta_0 = 0.65$ eV. In the present numerical simulation, the value $\lambda = 0.20$ is used. Without the impurities it gives $| y_n | = 0.0793$ Å and reproduces the same $\Delta_0 = 0.65$ eV. We compare the simulation results of a SSH system with the CPA results of a TLM system, both having the same Δ_0 but not necessarily the same λ. The CPA result is in a remarkable agreement with the above result, in spite of the fact that within the CPA a uniform order parameter is assumed.

Using the energy eigenvalues, we define the inverse level spacing d_μ^ν by

$$d_\mu^\nu = \begin{cases} \dfrac{1}{\varepsilon_{\mu+1}^\nu - \varepsilon_\mu^\nu} & \text{if } \mu = 1 \text{ and } N/2+1, \\ \dfrac{1}{\varepsilon_\mu^\nu - \varepsilon_{\mu-1}^\nu} & \text{if } \mu = N/2 \text{ and } N, \\ \dfrac{2}{\varepsilon_{\mu+1}^\nu - \varepsilon_{\mu-1}^\nu} & \text{otherwise,} \end{cases} \tag{3.1}$$

where ε_μ^ν is the μth eigenvalue of the νth sample. The spacings are associated with the level spacings of valence and conduction bands separately; the energy gap between both bands is not included. In Figs. 4(a), 4(b), and 4(c), we plot $N \times N_{\rm sa}$ points $(\varepsilon_\mu^\nu, d_\mu^\nu/N)$ for $1 \le \mu \le N$ and $1 \le \nu \le N_{\rm sa}$, for $\theta/2\pi$ =0, 0.25 and 0.5, respectively.

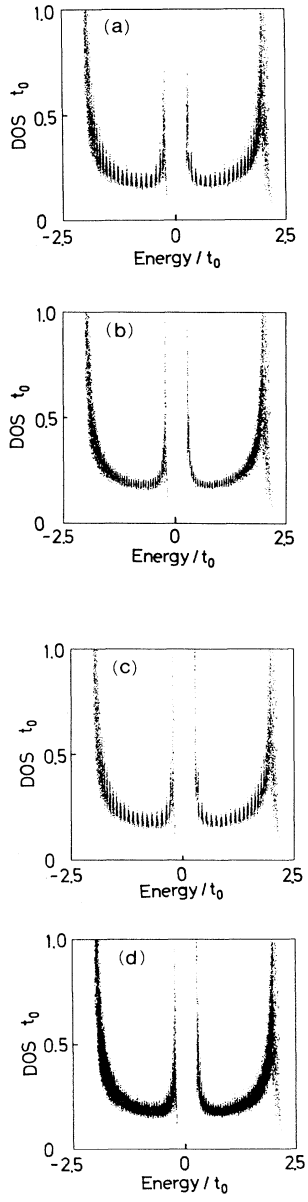

FIG. 4. Density of states per site of a system with site-type impurities. The abscissa is ε_μ and the ordinate d_μ/N. The impurity strength is $I_s = 0.4t_0$ and the concentration $c = 0.08$. (a) is for $\theta = 0$, (b) for $\theta/2\pi = 0.25$, and (c) is for $\theta/2\pi = 0.5$. The figure for $\theta/2\pi = 0.75$ almost coincides with (b). (d) is the superposition of the four figures. A remnant of an impurity band is seen at the top of the valence band.

The data points cluster around the eigenvalues of the impurity-free system. This clustering implies that finite-size effects remain. Due to the randomness, each cluster has a nonvanishing width. When θ is varied, each cluster moves according to the change in the eigenvalues, as illustrated in Figs. 2(b) and 2(c). The clusters at the edges of the valence and conduction bands do not move to the same amount as those in the middle regions of both bands. This is due to two effects: one is that the inverse level spacing is larger at the edges of bands than at the band centers. The other is that the disorder effect tends to localize the wave functions stronger at the band edges than at the band centers. Superposition of the four sets of plots for $\theta/2\pi = 0, 0.25, 0.5$, and 0.75 gives Fig. 4(d). The result looks continuous. This means that we have eliminated the finite-size effects and a statistical average has been performed successfully. Since $N_{\rm sa}$ is large enough, we can expect that Fig. 4(d) represents the density of states per site. A similar data analysis has been performed in Ref. 17. Above the tops of the valence and conduction bands, the density of states has tails in the energy gap and the higher energy region, respectively. These are remnants of the isolated impurity bands which have been obtained in the CPA analysis at low concentrations. The number of states in these tails is very small. If we would have tried to obtain the density of states by counting the number of states whose energies are in a given energy interval, we would have missed the tail structures.

Figure 5(a) shows the detailed plots of Fig. 4(d) close to the energy gap. Figure 5(b) is the result by the CPA. The two results agree well, though the CPA analysis has been made assuming a uniform order parameter.

The same calculation is performed for $I_s = 1.0t_0$ and $c = 0.03$. The density of states is shown in Fig. 6(a), close to the energy gap. The tail becomes broader and there may be a fine structure at the top of the valence band. Figure 6(b) shows the corresponding CPA result for $J = 0.5t_0$ and $c_{\rm CPA} = 0.06$. An overall similarity is evident. Positions of the peaks agree well. However, the fine structure is not reproduced in the CPA. This is a well-known limitation of the single-site approximation of the CPA, which appears for sufficiently strong disorder potential.[18]

IV. BOND-TYPE IMPURITIES

A. *Cis*-type doping

In the *cis*-type impurity Hamiltonian (2.13), its strength is taken to be $I_b = 0.2t_0$. As shown in the CPA analysis[1,2] the product $I_b\Delta$ is positive for the stable solution. We thus take a positive y_0, that is, $y_0 = 0.1$ Å. The concentration is $c = 0.08$.

A typical solution with $\theta = 0$ gives the smoothed dimerization amplitude in Fig. 7(a). It increases around each impurity. There are two types of deformation patterns. One of them is short ranged and is associated with a long bond. The other has a longer tail and is related to a short bond. This has been discussed already in Ref. 19. Figure 7(b) shows the electron density. It has a ho-

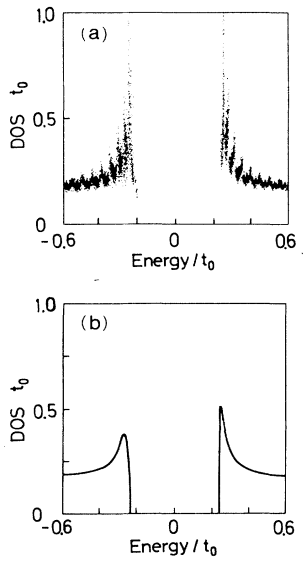

FIG. 5. (a) shows the details of Fig. 4(d) around the energy gap. In (b) the result of the CPA calculation is shown for $J = 0.2t_0$ and $c_{\rm CPA} = 0.16$, corresponding to the parameters in Fig. 4.

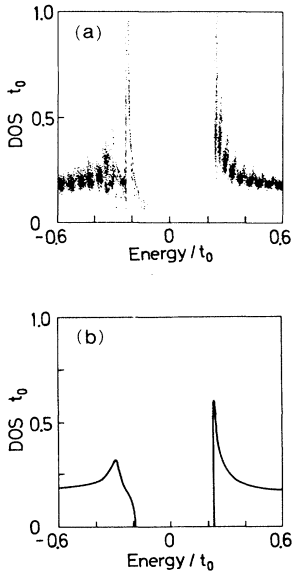

FIG. 6. (a) Density of states per site of a system with site-type impurities with $I_s = 1.0t_0$ and $c = 0.03$. In (b) the CPA result is shown for $J = 0.5t_0$ and $c_{\rm CPA} = 0.06$.

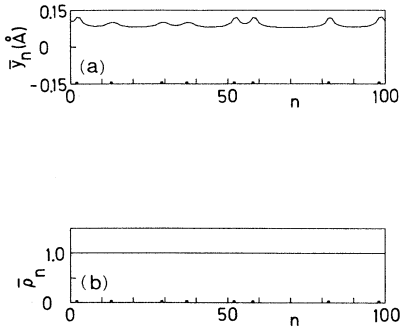

FIG. 7. (a) The smoothed dimerization amplitude $\bar{y}_n$ and (b) the smoothed electron-density distribution $\bar{\rho}_n$ for a typical sample with bond-type (*cis*-type) impurities. The impurity strength is $I_b = 0.2t_0$, and the concentration $c = 0.08$. The phase θ is zero. Positions of the impurities are indicated by the squares on the abscissa. The electron-hole symmetry results in a homogeneous distribution.

mogeneous distribution, since there is the electron-hole symmetry. Figure 8(a) shows $|\psi_{51}(n)|^2$ and Fig. 8(b) is $|\psi_{52}(n)|^2$. They are the two states at the bottom of the conduction band. The electron-hole symmetry results in the fact that each of $|\psi_\mu(n)|^2$ for the valence band ($\mu = 1$–50) is identical with a corresponding $|\psi_{101-\mu}(n)|^2$ for the conduction band. We find that the wave functions near the energy gap have large amplitudes in the impurity-free regions. Around each impurity, $\bar{y}_n$ becomes larger. So, the local energy gap around the impurity increases. The local energy gap becomes relatively smaller in the impurity-free regions. Consequently, the wave functions of the states near the energy gap tend to have larger amplitudes in the impurity-free regions.

The averaging procedure is performed over the N sites and $N_{\rm sa}$ samples to give $\langle | y_n | \rangle = 0.0902$ Å. This yields $\Delta = 0.740$ eV $= 0.296t_0$ in the TLM model. The CPA analysis[2] has given $\Delta = 0.765$ eV $= 0.306t_0$ for $I \equiv U_b/2a = 0.2t_0$ and $c_{\rm CPA} = 0.16$. The two values agree well, but the agreement is not so good as with the site-type impurities. The bond alternation y_n is modulated in first order with respect to I_b but in second order with respect to I_s. So, the spatial variation of y_n, which has not been taken into account in the CPA, would be more important in the system with bond-type impurities.

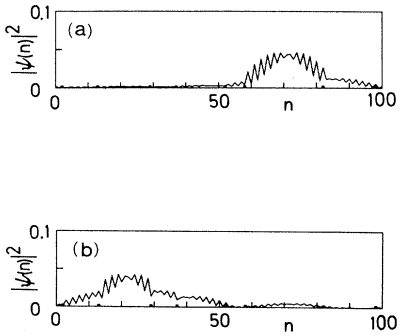

FIG. 8. Magnitude of the wave functions $|\psi_\mu(n)|^2$ for the typical sample in Fig. 7. (a) is for $\mu = 51$ and (b) for $\mu = 52$ (the bottom of the conduction band).

The density of states is shown in Fig. 9(a), after the superposition of the plots with $\theta/2\pi = 0$, 0.25, 0.5, and 0.75. It is symmetric because of the electron-hole symmetry. There are remnants of impurity bands, one at the bottom of the valence band, the other at the top of the conduction band, and no remnant in the energy gap.

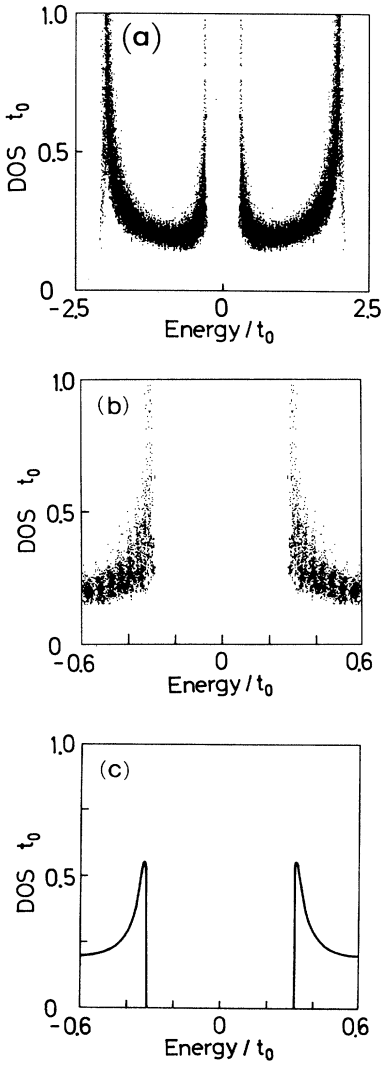

FIG. 9. Density of states per site of a system with bond-type (*cis*-type) impurities. The impurity strength is $I_b = 0.2t_0$ and the concentration $c = 0.08$. (a) is the superposition of the four corresponding figures with $\theta/2\pi = 0$, 0.25, 0.50, and 0.75. Remnants of two impurity bands are seen at the bottom of the valence band and at the top of the conduction band. (b) shows details around the energy gap region. In (c) the CPA result is shown with $I = 0.2t_0$ and $c_{\rm CPA} = 0.16$.

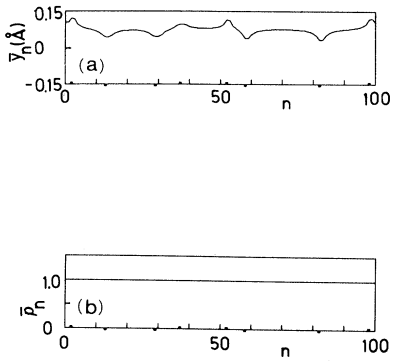

FIG. 10. (a) The smoothed dimerization amplitude $\bar{y}_n$ and (b) the smoothed electron-density distribution $\bar{\rho}_n$ for a typical sample with bond-type impurities and compensated doping. The impurity strength is $I_b = 0.2t_0$ and the concentration $c = 0.08$. The phase θ is zero. Positions of the positive impurities are indicated by the squares above the abscissa, and those of the negative impurities by the square below it. The homogeneous distribution is the consequence of the electron-hole symmetry.

Figure 9(b) shows the detailed plots of the region close to the gap. Figure 9(c) is the corresponding CPA result. The overall agreement is remarkable.

B. Compensated doping

The compensated doping is represented by the impurity Hamiltonian (2.15). We take the strength $I_b = 0.2t_0$. The CPA analysis[4] has shown that the sign of the order parameter is irrelevant. We thus take a positive y_0 (=0.1 Å). The impurity concentration is taken to be $c = 0.08$. There are as many impurities with I_b as impurities with $-I_b$.

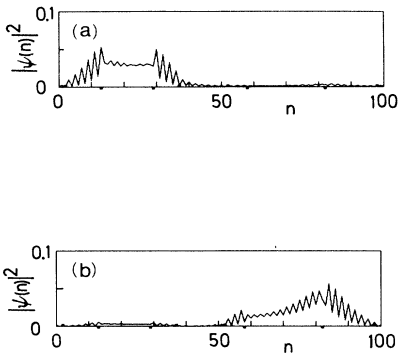

FIG. 11. Magnitude of the wave functions $|\psi_\mu(n)|^2$ for the typical sample in Fig. 10. (a) is for $\mu = 51$ and (b) for $\mu = 52$ (the bottom of the conduction band).

A typical sample with $\theta = 0$ gives the smoothed dimerization amplitude in Fig. 10(a). The locations of positive and negative impurities are denoted by squares above and below the abscissa, respectively. Around a positive impurity, the amplitude increases, while at a negative impurity, it decreases. We find the two types of the deformation patterns again. The pattern in the decrease around the negative impurities has just the same shape with that of the increase around positive impurities. Fig. 10(b) shows the electron density. It is distributed homogeneously just as in the case of *cis*-type doping. Figure 11(a) shows $|\psi_{51}(n)|^2$ and Fig. 11(b) $|\psi_{52}(n)|^2$. They are the two states at the bottom of the conduction band.

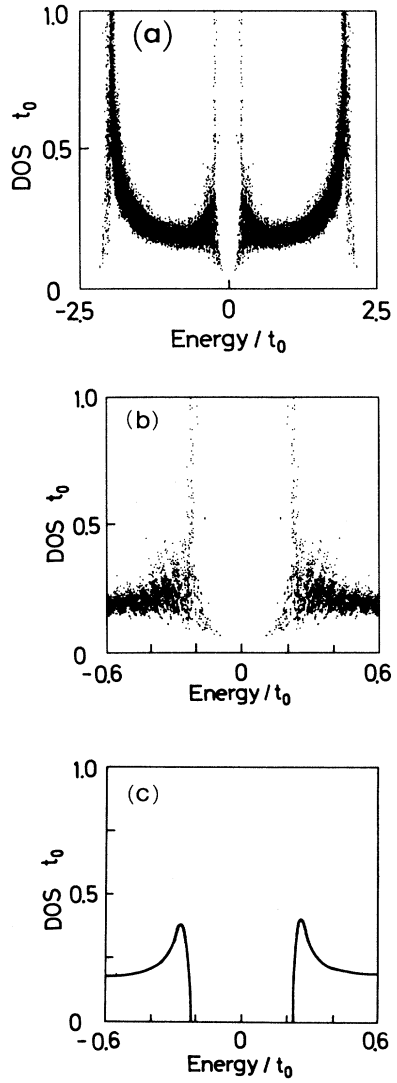

FIG. 12. Density of states per site of a system with bond-type impurities and compensated doping. The impurity strength is $I_b = 0.2t_0$ and the concentration $c = 0.08$. (a) is composed of the superposition of four plots for $\theta/2\pi = 0$, 0.25, 0.50, and 0.75. There are remnants of impurity bands at the bottom and the top of both bands. (b) shows details around the energy gap region. In (c) the CPA result is shown with $I = 0.2t_0$ and $c_{\mathrm{CPA}} = 0.16$.

The local energy gap increases around a positive impurity, while it decreases at a negative impurity. So, the states near the energy gap tend to have large amplitudes around negative impurities. The wave functions near the energy gap have a property common with *cis*-type impurities: they have large amplitudes in regions where the order parameter is small.

Averaging y_n over N sites and $N_{\rm sa}$ samples with $N_{\rm sa} = 100$, we get $\langle | y_n | \rangle = 0.0756$ Å and $\Delta = 0.620$ eV $= 0.248t_0$. The CPA calculation[4] has given $\Delta = 0.648$ eV $= 0.259t_0$ for $I = 0.2t_0$ and $c_{\rm CPA} = 0.16$. Thus, we confirm the decrease of the order parameter in the compensated doping, which has been predicted in Ref. 4.

The density of states is shown in Fig. 12(a). There are four remnants of impurity bands: two of them in the energy gap, another at the bottom of the valence band, and the last at the top of the conduction band. Figure 12(b) is the detailed drawing in the region close to the energy gap. In Fig. 12(c) we show the CPA result for comparison. It reproduces the gross structures. In Ref. 4 it has been discussed that two impurity bands in the energy gap are originated from the negative impurities when the order parameter is positive. This also agrees with the above discussion that the wave functions near the energy gap have large amplitudes around negative impurities.

V. DISCUSSIONS

We have shown that there are remarkable agreements between the CPA results in the TLM model and the numerical results in the SSH model. The averaged order parameters agree well with the CPA results. The agreement is better for a system with site-type than for bond-type impurities. The effects of the spatial variation of the order parameter would be more apparent in the bond-type system. We find distinctive features in the density of states of the valence or the conduction band. In some cases there is a tail in the energy gap, which we have related to the presence of an impurity band. In other cases, there is not such a tail. These tails appear only in cases where the CPA predicts an isolated impurity band for low enough concentrations.

Spatial distributions of the wave functions near the energy gap have properties similar to the ones one would expect for impurity bands. When a band has a tail, the wave functions near this edge have large amplitudes around impurities. The valence band in Fig. 5(a) has such a tail. Consequently the wave functions ψ_{49} and ψ_{50} have large amplitude around the impurities in Figs. 3(a) and 3(b). In Fig. 12(b), both valence and conduction bands have this tail, and the wave functions ψ_{51} and ψ_{52} are large at the impurities sites, as shown in Fig. 11. The functions ψ_{50} and ψ_{49} have the same structure, since the particle-hole symmetry holds. If there is no such tail, the wave functions localize in the impurity-free regions. There is no tail for the conduction band in Fig. 5(a), and the wave functions ψ_{51} and ψ_{52} are in the impurity-free regions as shown in Figs. 3(c) and 3(d). The two bands in Fig. 9(b) do not have a tail, and the wave functions ψ_{51} and ψ_{52} are in the impurity-free regions in Figs. 8(a) and 8(b) as well. There is again particle-hole symmetry. This is quite reasonable since the impurity bands originate from the localized states around the impurities.

In the present paper, we have considered the impurity concentrations of the order of several percent. According to the CPA, the impurity bands in the energy gap are connected to the conduction and/or valence bands at this concentration. At lower concentrations, the impurity bands would be isolated. In order to simulate such a system with a low concentration, we need a large system to get a large number of eigenstates. Therefore, we have not performed such a calculation. However, we believe that the CPA calculations describe the global features of the density of states in such a low-concentration system also.

When the impurity concentration becomes higher, we have a rapidly increasing number of samples in which solitons and polarons present. The energy-level structure then becomes much more complicated as well as the lattice configuration. With solitons and polarons present, the CPA has to be generalized to take into account the spatial variation of the order parameter. This poses a very interesting problem.

ACKNOWLEDGMENTS

Fruitful discussions with Y. Ono, T. Ohtsuki, and K. Yonemitsu are acknowledged. This work has been partially supported by Deutsche Forschungsgemeinschaft through Sonderforschungsbereich 213 (TOPOMAK, Bayreuth). Numerical calculations have been performed on Fujitsu FACOM M-380Q of ICEPP (International Center for the Elementary Particle Physics), University of Tokyo, and on Hitachi HITAC S-820 in the computer center of Institute for Molecular Science, Okazaki National Research Institutes, Japan.

[1] K. Harigaya, Y. Wada, and K. Fesser, Phys. Rev. Lett. **63**, 2401 (1989); *ibid.* **65**, 806(R) (1990).
[2] K. Harigaya, Y. Wada, and K. Fesser, Phys. Rev. B **42**, 1268 (1990).
[3] K. Harigaya, Y. Wada, and K. Fesser, Phys. Rev. B **42**, 1276 (1990).
[4] K. Harigaya, J. Phys. Soc. Jpn. **59**, 1348 (1990).
[5] K. Harigaya, Y. Wada, and K. Fesser, Phys. Rev. B **42**, 11 303 (1990).
[6] K. Harigaya, Y. Wada, and K. Fesser, in *Strongly Coupled Plasma Physics*, edited by S. Ichimaru (Elsevier, New York, 1990), p. 255.

[7]W. -P. Su, J. R. Schrieffer, and A. J. Heeger, Phys. Rev. B **22**, 2099 (1980).
[8]H. Takayama, Y. R. Lin-Liu, and K. Maki, Phys. Rev. B **21**, 2388 (1980).
[9]S. Kivelson, T. K. Lee, Y. R. Lin-Liu, I. Peschel, and L. Yu, Phys. Rev. B **25**, 4173 (1982).
[10]X. Sun, C. Wu, and X. Shen, Solid State Commun. **56**, 1039 (1985).
[11]K. A. Chao and Y. Wang, J. Phys. C **18**, 1127 (1985).
[12]A. Terai and Y. Ono, J. Phys. Soc. Jpn. **55**, 213 (1986).
[13]C. Wu and X. Sun, Phys. Rev. B **33**, 8772 (1986); R. J. Cohen and A. J. Glick, *ibid.* **36**, 2907 (1987); K. Yonemitsu and Y. Wada, J. Phys. Soc. Jpn. **56**, 4400 (1987).
[14]Y. Ono, K. Iwano, A. Terai, Y. Ohfuti, and Y. Wada, J. Phys. Soc. Jpn. **58**, 2450 (1989); K. Iwano, Y. Ono, A. Terai, Y. Ohfuti, and Y. Wada, *ibid.* **58**, 4048 (1989).
[15]J. T. Edwards and D. J. Thouless, J. Phys. C **5**, 807 (1972); D. C. Licciardello and D. J. Thouless, *ibid.* **8**, 4157 (1975).
[16]S. A. Brazovskii and N. N. Kirova, Pis'ma Zh. Eksp. Teor. Fiz. **33**, 6 (1981) [JETP Lett. **33**, 4 (1981)].
[17]L. Ye, A. J. Freeman, D. E. Ellis, and B. Delley, Phys. Rev. B **40**, 6277 (1989).
[18]See, for example, F. Yonezawa, and K. Morigaki, Suppl. Prog. Theor. Phys. **53**, 1 (1973); J. M. Ziman, *Models of Disorder* (Cambridge University Press, Cambridge, England, 1979), Chap. 9.
[19]S. R. Phillpot, D. Baeriswyl, A. R. Bishop, and P. S. Lomdahl, Phys. Rev. B **35**, 7533 (1987).